HAL open science

Atomic structure of Lanreotide nanotubes revealed by cryo-EM

Laura Pieri, Fengbin Wang, Ana-Andreea Arteni, Matthijn Vos, Jean-Marie Winter, Marie-Hélène Le Du, Franck Artzner, Frédéric Gobeaux, Pierre Legrand, Yves Boulard, et al.

To cite this version:

Laura Pieri, Fengbin Wang, Ana-Andreea Arteni, Matthijn Vos, Jean-Marie Winter, et al.. Atomic structure of Lanreotide nanotubes revealed by cryo-EM. Proceedings of the National Academy of Sciences of the United States of America, 2022, 119 (4), pp.e2120346119. 10.1073/pnas.2120346119 . hal-03541906

HAL Id: hal-03541906

https://hal.science/hal-03541906v1

Submitted on 31 May 2022

HAL is a multi-disciplinary open access archive for the deposit and dissemination of scientific research documents, whether they are published or not. The documents may come from teaching and research institutions in France or abroad, or from public or private research centers.

L'archive ouverte pluridisciplinaire **HAL**, est destinée au dépôt et à la diffusion de documents scientifiques de niveau recherche, publiés ou non, émanant des établissements d'enseignement et de recherche français ou étrangers, des laboratoires publics ou privés.

Distributed under a Creative Commons Attribution - NonCommercial - NoDerivatives 4.0 International License

Atomic structure of Lanreotide nanotubes revealed by cryo-EM

Laura Pieri[a,1], Fengbin Wang[b,1], Ana-Andreea Arteni[a], Matthijn Vos[c], Jean-Marie Winter[c], Marie-Hélène Le Du[a], Franck Artzner[d], Frédéric Gobeaux[a,e], Pierre Legrand[f], Yves Boulard[a], Stéphane Bressanelli[a], Edward H. Egelman[b,2], and Maité Paternostre[a,2]

[a]CEA, CNRS, Université Paris-Saclay, Institute for Integrative Biology of the Cell (I2BC), 91198 Gif-sur-Yvette, France; [b]Department of Biochemistry and Molecular Genetics, School of Medicine, University of Virginia, Charlottesville, VA 22908; [c]Nanoimaging Core Facility, Institut Pasteur, 75015 Paris, France; [d]Institute de Physique de Rennes, Université Rennes 1, 35000 Rennes, France; [e]Commissariat à l'Energie Atomique, CNRS, Nanosciences et Innovation pour les Matériaux, la Biomédecine et L'Energie, LIONS, Université Paris-Saclay, 91191 Gif-sur-Yvette, France; and [f]Synchrotron SOLEIL, 91192 Gif-sur Yvette, France

Contributed by Edward H. Egelman; received November 7, 2021; accepted December 13, 2021; reviewed by Javier Montenegro and Joel Schneider

Functional and versatile nano- and microassemblies formed by biological molecules are found at all levels of life, from cell organelles to full organisms. Understanding the chemical and physicochemical determinants guiding the formation of these assemblies is crucial not only to understand the biological processes they carry out but also to mimic nature. Among the synthetic peptides forming well-defined nanostructures, the octapeptide Lanreotide has been considered one of the best characterized, in terms of both the atomic structure and its self-assembly process. In the present work, we determined the atomic structure of Lanreotide nanotubes at 2.5-Å resolution by cryoelectron microscopy (cryo-EM). Surprisingly, the asymmetric unit in the nanotube contains eight copies of the peptide, forming two tetramers. There are thus eight different environments for the peptide, and eight different conformations in the nanotube. The structure built from the cryo-EM map is strikingly different from the molecular model, largely based on X-ray fiber diffraction, proposed 20 y ago. Comparison of the nanotube with a crystal structure at 0.83-Å resolution of a Lanreotide derivative highlights the polymorphism for this peptide family. This work shows once again that higher-order assemblies formed by even well-characterized small peptides are very difficult to predict.

peptide assemblies | helical polymers | three-dimensional reconstruction

Peptide assemblies forming hydrogels or fibrils have been used for biomedical applications, such as drug delivery, cell culture, vaccines, and tissue regeneration (1). Peptides are indeed potentially important molecules as drugs, but they are generally very sensitive to enzymatic degradation in vivo. Many strategies have been devised to improve the stability of peptides, such as the incorporation of unnatural amino acids, but also the use of the peptide in the form of assemblies to slow down the degradation kinetics (2). Both of these strategies were employed 20 y ago for Lanreotide, a somatostatin analog used against acromegaly and now also for certain forms of neuroendocrine cancers (3). In addition, the self-assembled formulation, called Somatuline autogel, when injected under the skin, not only protects the peptide from degradation, but allows a slow and continuous release for a month (4, 5). This sustained-release formulation consists of only water and peptide, because the biologically active molecule self-assembles into nanotubes.

Lanreotide is an octapeptide whose sequence is [H_2N-Nah_1-cyclo(Cys_2-Tyr_3-D-Trp_4-Lys_5-Val_6-Cys_7)-Thr_8-NH2]. Of the eight side chains of Lanreotide, three are aromatics (Fig. 1*G*). Two of these aromatic side chains are unnatural, such as a D-naphthylalanine (Nah) and a D-Tryptophan (DTrp), the third aromatic being a tyrosine (Tyr). The peptide also carries two positive charges, on the N terminus and on Lys, C-terminal end being amidated and neutral. Lanreotide has a disulfide bridge locking it into a β-hairpin conformation as seen in a crystal structure of a Lanreotide derivative (Fig. 1*G*). The peptide has two aliphatic side chains, one hydrophobic (Val) and the other hydrophilic (Thr). The three aromatic side chains are segregated on one of the branches of the β-hairpin (Fig. 1*G*).

At room temperature and at lower concentrations of Lanreotide in pure water (up to ∼20 mM), a monomer–dimer equilibrium is established with a high K_d (∼5 mM) (6). Above this concentration and up to about 150 mM, Lanreotide self-assembles and forms very long (a few hundreds of micrometers) hollow nanotubes that pack together hexagonally (6, 7). Using a multimethodological approach (optical microscopy under crossed polarizers, low-resolution electron microscopy after negative staining, or freeze-fracture, X-ray fiber diffraction, vibrational spectroscopies [ATR-FTIR and Raman]), a molecular model of the nanotubes was proposed (8).

The structure published in 2003 (8) proposed that the two nonequivalent layers forming the nanotube walls were formed from the lateral association of β-sheets, therafter referred to as "protofilaments." In between the protofilaments, the side chains involved in the close contacts were different on the external and luminal layer (i.e., the Lys for the external layer and the DTrp for the luminal one). In this model, the size of the side chains making the close contact between the protofilaments determined the radius of curvature of the nanotubes: increasing the steric hindrance of the close contact between the protofilaments of the luminal layer should increase the diameter of the nanotubes,

Significance

The spectacular developments in cryoelectron microscopy involving new cameras, new microscopes, and new software make it possible today to routinely determine the atomic structures of a large range of molecular assemblies. This has allowed us to solve the atomic structure of nanotubes formed from a peptide, Lanreotide. Its gel, Somatuline, is used as a synthetic growth hormone inhibitor in the treatment of both acromegaly and cancers. The self-assembled nanotube results in a slow release form of the peptide, important pharmacologically. The nanotube structure shows an unexpected complexity and highlights the still unpredictable chemical and physicochemical determinants driving peptide self-assembly.

Author contributions: M.P. designed research; L.P., A.-A.A., M.V., J.-M.W., M.-H.L.D., F.G., and P.L. performed research; L.P., F.W., F.A., P.L., Y.B., S.B., E.H.E., and M.P. analyzed data; and L.P., F.W., Y.B., S.B., E.H.E., and M.P. wrote the paper.

Reviewers: J.M., Santiago de Compostela University; and J.S., National Cancer Institute.

The authors declare no competing interest.

This article is distributed under Creative Commons Attribution-NonCommercial-NoDerivatives License 4.0 (CC BY-NC-ND).

[1]L.P. and F.W. contributed equally to this paper.

[2]To whom correspondence may be addressed. Email: egelman@virginia.edu or maite.paternostre@i2bc.paris-saclay.fr.

This article contains supporting information online at http://www.pnas.org/lookup/suppl/doi:10.1073/pnas.2120346119/-/DCSupplemental.

Published January 18, 2022.

BIOPHYSICS AND COMPUTATIONAL BIOLOGY

Downloaded from https://www.pnas.org by Universite de Rennes 1 on May 31, 2022 from IP address 129.20.30.54.

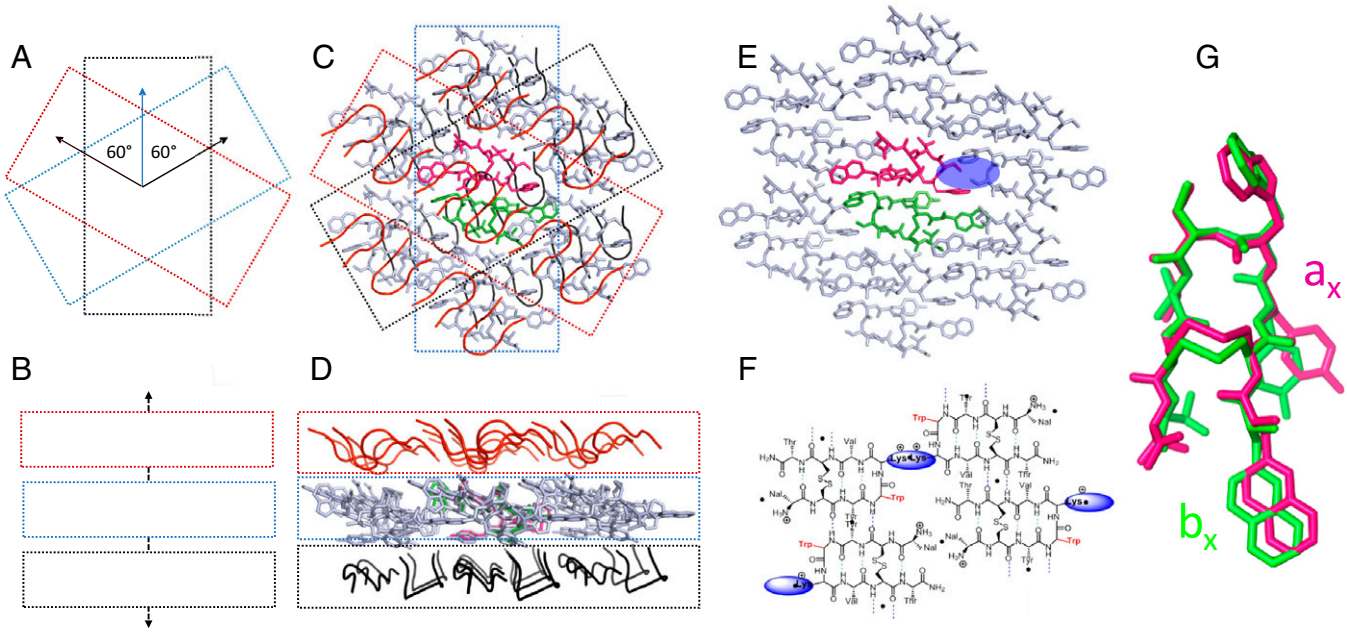

Fig. 1. Crystal structure of the Lanreotide derivative Lan-dap5. Schematic representation of the crystalline stack formed by successive monolayers of peptides rotated by 60° with respect to each other: (*A*) top and (*B*) side views. Details of the peptide monolayers: (*C* and *E*) top views and (*D*) side view. (*C* and *D*) Superposition of three monolayers of peptides. The peptides in the middle layer are shown in a stick representation, while just the peptide backbones are shown for the surrounding layers. (*E*) Detailed structure of one peptide layer. Molecules a_x (magenta) and b_x (green) are stacked head-to-tail in the asymmetric unit of the crystal. The blue ellipsoid highlights the close proximity of diaminopropionic acid side chains (replacing Lys in Lan-dap5) between adjacent β-sheets. (*F*) The molecular packing proposed in 2003 for the external peptide layer of the lanreotide nanotube wall. The putative Lys-Lys close contacts between adjacent β-sheets are highlighted by the blue ellipsoids (adapted from ref. 10). (*G*) superposition of the two conformations a_x (magenta) and b_x (green) of Lan-dap5 present in the asymmetric unit.

whereas increasing the steric hindrance of the close contact between the protofilaments of the external layer should decrease it. This hypothesis based on the geometrical model was indeed experimentally verified (9, 10).

Lan-dap5 is a Lanreotide derivative in which the aliphatic chain of Lys (four CH2 groups) at position 5 has been shortened by replacing it with a diaminopropionic acid (one CH2 group) (*SI Appendix*, Fig. S1). For this derivative that forms the largest diameter nanotubes (about 32 nm), it was observed that under different conditions the peptide can form microcrystals whose infra-red spectra are similar to those from nanotubes (10). It was therefore assumed that the crystals resulted from the stacking of planar peptide bilayers whose structure was similar to that of the nanotube walls.

In the present work, we compare two new structures: the X-ray crystal structure of the Lanreotide derivative Lan-dap5 at 0.83-Å resolution and the cryo-EM structure of the Lanreotide nanotube at 2.5 Å resolution. The crystal structure shows an organization close to that of the external layer of the nanotube molecular model proposed in 2003. However, the actual high-resolution cryoelectron microscopy (cryo-EM) structure of the Lanreotide nanotube exhibits different molecular conformations and packing. In addition to showing an unsuspected polymorphism for Lanreotide, the atomic structure of the nanotubes again shows the power of the cryo-EM approach in studying peptide assemblies and the difficulty in predicting the way that small peptides self-assemble, due in part to the multiple conformations a peptide can adopt within assemblies (11).

Results

Crystal Structure of Lan-Dap5 Derivative. It was previously shown that depending on the method of preparing the sample, the Lan-dap5 lanreotide derivative could either self-assemble into 32-nm diameter nanotubes (thermal annealing) or form microcrystals (preparation at room temperature) (10). Therefore, after improving the size of the crystals, we determined the structure of Lan-dap5 by X-ray crystallography with a final resolution of 0.83 Å (Table 1).

The crystal is formed by the stacking of peptide layers as was originally imagined for the nanotube. The crystal structure shows a stacking of monolayers of peptide, each successive layer being rotated by 60° along the 6_1 c-axis of the crystal (Fig. 1 *A–D* and Table 1). The crystal packing is compatible with the one proposed (8) for the external layer of the nanotube walls (Fig. 1 *E* and *F*). The asymmetric unit contains two head-to-tail Lan-dap5 molecules forming a continuous antiparallel β-sheet as in the 2003 nanotube model. The two-dimensional (2D) lattice parameters of the asymmetric unit dimer (Table 1) are compatible with the previous molecular model (a = 20.7 Å, b = 20.8 Å, γ = 119°). The surface occupied by the asymmetric unit dimer is compatible with the previous molecular model, and the two monomers a_x and b_x are slightly different from each other (Fig. 1*G*) with a pseudo C_2 symmetry. Looking at the close contacts between juxtaposed β-sheets, the proximity of dap5 dipropionic acid side chains from two adjacent sheets is completely consistent with the hypothesis that the Lys side chains make the close contacts in the external peptide layer in Lanreotide nanotubes (Fig. 1 *E* and *F*). It must be kept in mind, however, that Lan-dap5 is a derivative of Lanreotide and the structure comes from a crystal grown in presence of ethanol. Indeed, two molecules of ethanol are visible between the two dap5 and groups of aromatic side chains.

Cryo-EM Nanotube Helical Reconstruction: Chirality and Hand. Lanreotide self-assembles into nanotubes of well-defined and homogeneous diameter. Despite the high viscosity of the sample, abundant nanotubes within very satisfactory ice could be

Downloaded from https://www.pnas.org by Universite de Rennes 1 on May 31, 2022 from IP address 129.20.30.54.

Table 1. Data collection and refinement statistics

Data collection and refinement	
Wavelength (Å)	0.7999/0.78971
Resolution range (Å)	15.78–0.825 (0.8597–0.825)
Space group	$P6_1$
Unit cell (*a*,*b*, *c* (Å) /α, β, γ °)	18.95 18.95 57.52/90 90 120
Total reflections	494,120 (6,053)
Unique reflections	11,006 (1,082)
Multiplicity	44.9 (5.6)
Completeness (%)	99.61 (96.44)
Mean I/σ(I)	91.68 (8.36)
Wilson B-factor	4.77
R_{merge}	0.02957 (0.1521)
R_{meas}	0.02985 (0.167)
R_{pim}	0.004002 (0.06557)
CC1/2	1 (0.98)
CC*	1 (0.995)
Reflections used in refinement	11,004 (1084)
Reflections used for R_{free}	1,102 (107)
R_{work}	0.0773 (0.1111)
R_{free}	0.0858 (0.1376)
CC (work)	0.994 (0.961)
CC (free)	0.987 (0.906)
Number of nonhydrogen atoms	179
RMS (bonds)	0.015
RMS (angles)	2.12
Ramachandran favored (%)	100.00
Ramachandran allowed (%)	0.00
Ramachandran outliers (%)	0.00
Rotamer outliers (%)	0.00
Clashscore	3.34
Average B-factor	4.73

Statistics for the highest-resolution shell are shown in parentheses. PDB ID code 7Q5G.

observed after vitrification. (*Material and Methods* and Fig. 2*A*). The homogeneity of the sample is easily recognized, as after particle picking and initial data processing ∼90% of the particles fall into 2D class averages with the same diameter (Fig. 2*B*).

The principal difficulties for getting a high-resolution helical reconstruction by cryo-EM are either related to the sample itself (homogeneity and quality of the vitrified sample and ice for cryo-EM imaging) or difficulties in the data analysis (e.g., ambiguities in the determination of helical symmetry) (12). In this case, the very small size of the peptide compared to the very large diameter of the assembly makes the determination of the correct helical symmetry more difficult. After searching by trial and error more than 50 possible helical symmetries based on the averaged power spectrum (*SI Appendix*, Fig. S2), the helical symmetry was determined to be an axial rise of 1.04 Å and a twist of ±26.2°. The correct hand of an EM map is often determined using a chiral part of the structure, usually an α-helix, which is not available here.

The final cryo-EM map has a resolution of 2.5 Å (Fig. 2 *C*–*E* and Table 2). Surprisingly, there are eight molecules in the helical asymmetric unit, which can be grouped in two main conformations (Figs. 2*D* and 3 *A*–*C*). In Fig. 2*D*, two molecules representative of the two main conformations are shown together with their corresponding EM map. They are distinguished by the orientation of the Nah side chain that caps the disulfide bridge for the "capped molecules" (in orange, hereafter referred to as "capped") and is oriented away from the disulfide bridge for the "away molecules" (in cyan, hereafter referred to as "away") (Fig. 2*D*). Between the two molecules, the map around the disulfide bridge is not similar. In particular, the density associated with the disulfide bridge of the molecule in the away conformation is lost. This loss is due to the known sensitivity of disulfide bonds to electron radiation (13), as can be seen by using a much lower dose (*SI Appendix*, Fig. S4). However, we find that the radiation damage is less than that found using microcrystal electron diffraction from a crystal (13). This may be due to the fact that it is difficult to separate actual radiation damage from increased B-factors in the crystallographic case. At any rate, our map illustrates that the sensitivity of the disulfide bond to electron radiation is dependent on its chemical environment, as the density of the disulfide bond for the capped molecules is more pronounced than for the away molecules.

Given that three-dimensional (3D) reconstructions in cryo-EM are made from 2D projection images where the absolute hand is lost, there is frequently an enantiomorphic ambiguity when reconstructing peptide assemblies or even proteins that do not contain α-helices. Here, the resolution of the map allows for the chirality of the map to be established, either by looking at α-carbons for the better-defined residues (Fig. 2*E*) or by

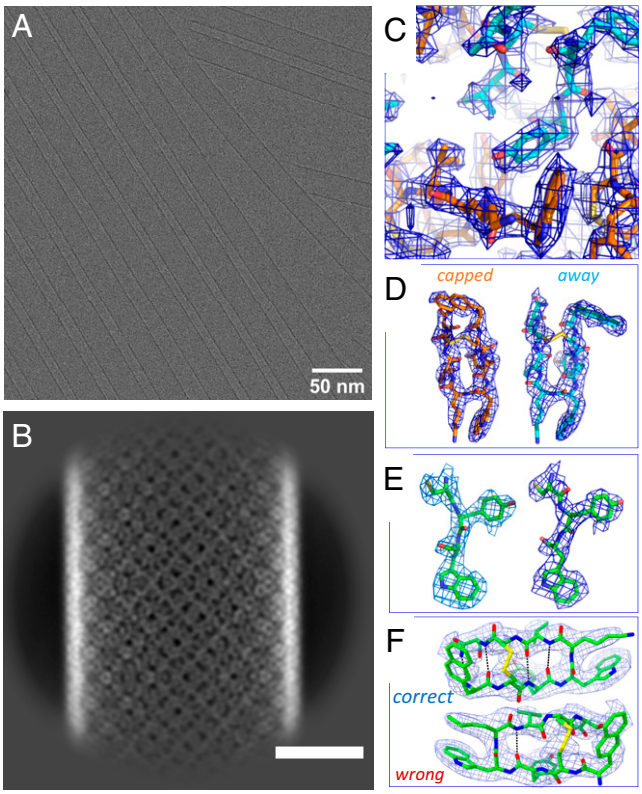

Fig. 2. Cryo-EM: analysis, density map and hand determination. (*A*) Cryo-EM image of Lanreotide nanotubes. (Scale bar, 50 nm.) (*B*) One representative 2D class average. (Scale bar, 10 nm.) (*C*) Close-up of the density map to show its quality. (*D*) Density maps for the two main conformations of Lanreotide within the helical asymmetric unit that differ by the position of the DNah side chains; that is, the capped molecule (orange carbons) and the away molecule (cyan carbons) (see *SI Appendix*, Fig. S3 for the density map of the asymmetric unit). (*E*) Determination of the correct hand for the structure of the nanotubes. Part of the Lanreotide model [Cys_2-Tyr_3-(D)-Trp_4 of a single molecule] is displayed after fitting into the correct map hand (*Left*) and into the inverse map hand (*Right*). Note the poor fit around the D-Trp_4 C_α in the inverse hand case, particularly for the carbonyl, C_β and side chain. In *D* and *E*, the map is displayed only around the selected atoms for clarity. (*F*) A further determination of the correct hand of the cryo-EM map can be made from examining the pattern of backbone hydrogen bonds. A single peptide is displayed after real-space refinement into the correct map hand (*Upper*) and into the mirrored map with the wrong hand (*Lower*). All of the expected antiparallel β-sheet hydrogen bonds only exist in the map with the correct hand.

BIOPHYSICS AND COMPUTATIONAL BIOLOGY

Downloaded from https://www.pnas.org by Universite de Rennes 1 on May 31, 2022 from IP address 129.20.30.54.

Table 2. Cryo-EM structure determination and model building parameters

Data collection and refinement	Parameter value
Data collection and processing	
Voltage (kV)	300
Electron exposure (e-/Å^2/frame)	1
No. of frames	60
Frames used for the analysis	2–40
Pixel size initial/after down-sampling (Å)	0.85/1.11
Defocus range (μm)	0.6–2.4
Extraction box size (pix)	512
Box size after down-sampling (pix)	392
Helical rise (Å)	1.04
Helical twist (°)	26.2
Map resolution (Å) (map:map FSC, cutoff 0.143)	2.5
Map sharpening B factor (Å^2)	−103.5
Initial number of segments	5,109,922
Final number of segments	2,264,921
Refinement and model validation*	
Model:map FSC (Å, cutoff 0.5)	2.5
RSCC	0.84
Bond lengths RMSD (Å)	0.011
Bond angles RMSD (°)	1.033
Clashscore	2.27
Poor rotamers (%)	0
Ramachandran favored (%)	100
Ramachandran outlier (%)	0
MolProbity score	1.00

*Values from PHENIX comprehensive validation (26). PDB ID code 7Q5A, EMD-13830, EMPIAR 10873.

modeling the pattern of backbone hydrogen bonds (Fig. 2*F*), permitting unambiguous assignment of the overall map hand.

Structure of the Nanotubes: Molecular Packing. The peptides are arranged in a monolayer almost radially to the axis of the nanotubes (Fig. 3*C*). Thus, the thickness of the nanotube is about the length of the peptide (i.e., 2 nm), consistent with the thickness previously suggested (8) (i.e., 1.8 nm). The asymmetric unit is composed of the eight molecules clustered into two nonequivalent tetramers (Fig. 3 *A*–*C*). Interestingly, those eight molecules are in slightly different environments and conformations within the nanotube.

As mentioned, the eight molecules can be grouped into two main capped and away conformations, depending on the Nah orientation: molecules a_c, b_c, g_c, and h_c are capped and c_a, d_a, e_a, f_a are away (Figs. 2*D* and 3*B* and *SI Appendix*, Fig. S3 in orange and cyan). Within a main conformation, the molecules are not equivalent and show subtle differences in the orientation of the side chains and especially Tyr, D-Trp, and Lys (Fig. 3*D* and *SI Appendix*, Table S1). Consequently, the environments of the molecules are all different (Fig. 3*E* and *SI Appendix*, Fig S5).

As expected, the β-hairpin conformation of the peptide introduces intramolecular antiparallel β-sheet H-bonds. With the same cutoff for assigning a polar contact between a main-chain nitrogen and carbonyl, three or four H-bonds are formed intramolecularly in capped molecules, while four or five are formed in away molecules, a further diagnostic of differences between the eight molecules. Interestingly, intermolecular H-bonds link all neighboring peptide backbones but in two distinct kinds of β-sheets: a_c-d_a-g_c-f_a-a_c-… and c_a-b_c-e_a-h_c–c_a-… These sheets extend for the length of the tube (Fig. 3 *F*–*H*). About 120 a_c-d_a-g_c-f_a or c_a-b_c-e_a-h_c molecules are required for the sheet to complete a 360° turn around the nanotube (*SI Appendix*, Fig. S6). This small average angle between two successive peptides along a sheet reflects the large radius of curvature of the nanotube. Moreover, the intermolecular H-bonds are alternatively antiparallel (Fig. 3 *F*–*H*, blue dots) and parallel (Fig. 3 *F*–*H*, pink dots) in both β-sheets (Fig. 3 *G* and *H*). The radial curvature is reflected only in slightly different lengths between the main-chain nitrogens and carbonyls and sometimes different reported numbers of intermolecular H-bonds (Fig. 3 *G* and *H*, compare e.g., a_c-d_a to g_c-f_a).

Finally, in Fig. 3*I* we compare the conformations of the molecules a_c and c_a, representative of the two conformational families present in the nanotubes, with molecule a_x of the crystal. The crystal conformation differs starkly from the two main conformations in the nanotube in that all three aromatic residues within the crystal (Fig. 1) have very different orientations than those found within the nanotube. This brings us to the role of the aromatic and aliphatic side chains in the stabilization of the nanotubes (Fig. 4).

Peptide Contacts and Roles of Side Chains. The segregation between aliphatic and aromatic residues already present at the monomer level is amplified in the nanotube wall (Fig. 4*A*). Aromatic clusters connect molecules into capped–away pairs (a_c-c_a, d_a-b_c, e_a-g_c, and h_c-f_a). In all four pairs, the two Tyr residues are positioned perpendicularly to each other indicating a strong interaction and the two DTrp are on either side of the Tyr pair (Fig. 4 *C*, *Bottom*). This aromatic network is extended by a single Nah from a third, capped molecule, to the DTrp of the capped molecule of the pair (e.g., the g_c Nah to the b_c DTrp in Fig. 4 *C*, *Bottom*). Two pairs are further connected by their four valine side chains (Fig. 4*C*), forming the aforementioned two tetramers $a_cc_ad_ab_c$ and $e_ag_ch_cf_a$ of the asymmetric unit. The Val side chains make up the center of a small hydrophobic core in each of the tetramers. However, van der Waals contacts are not made and while water is excluded, explaining the cohesion of the tetramers from the hydrophobic effect, there is a remaining hole in this core (Fig. 3*B*). Searching the PDB for similar valine clusters, we found four-residue groups including up to three valines, but always completed by a hydrophobic residue with a larger side chain, such as isoleucine or leucine. The other residues in the very center of the wall (i.e., the part totally excluded from water) are Tyr and the two Cys forming the disulfide bond (Fig. 4*B*).

Due to the radius of curvature of the nanotubes, the external surface is >20% larger than the luminal surface and indeed presents differences in terms of accessibility to the solvent (*SI Appendix*, Figs. S7 and S8). Yet, due to the alternate orientation of the peptides through the monolayer forming the wall of the nanotube, the nanotube alternately presents the same residues to water on its outer and luminal surfaces, and the same number of capped and away conformations (Fig. 3 *G* and *H*). However, molecules c_a, d_a, g_c, and h_c systematically have their C terminus and N terminus oriented outwards while molecules a_c, b_c, e_a, and f_a direct them toward the lumen. Thus, the differences in molecular packing on the outer and luminal surfaces are entirely due to the smaller differences between the eight distinct conformations. Fig. 4*B* shows the distribution of side chains from the surface to the center of the Lanreotide monolayer. The two side chains, Lys and DTrp, are the most exposed and in contact with water (Fig. 4 *B* and *C*). Remarkably, the aliphatic part of the Lys side chain is aligned with the aromatic rings of DTrp (see also Fig. 2*D* and *SI Appendix*, Fig S9). The hydrophilic parts of the two residues are in direct contact with water.

Nah (together with Val) is the most hydrophobic residue in the Lanreotide sequence, but because Nah is the N-terminal residue, it is very close to the nanotube surface. The Nah side chain is, however, recessed from water in both capped and away conformations and on both the outer and luminal sides, with mostly the main-chain positive charge exposed. Nearby and at the edge of the tetramer's hydrophobic core is the C-terminal Thr, that

Downloaded from https://www.pnas.org by Universite de Rennes 1 on May 31, 2022 from IP address 129.20.30.54.

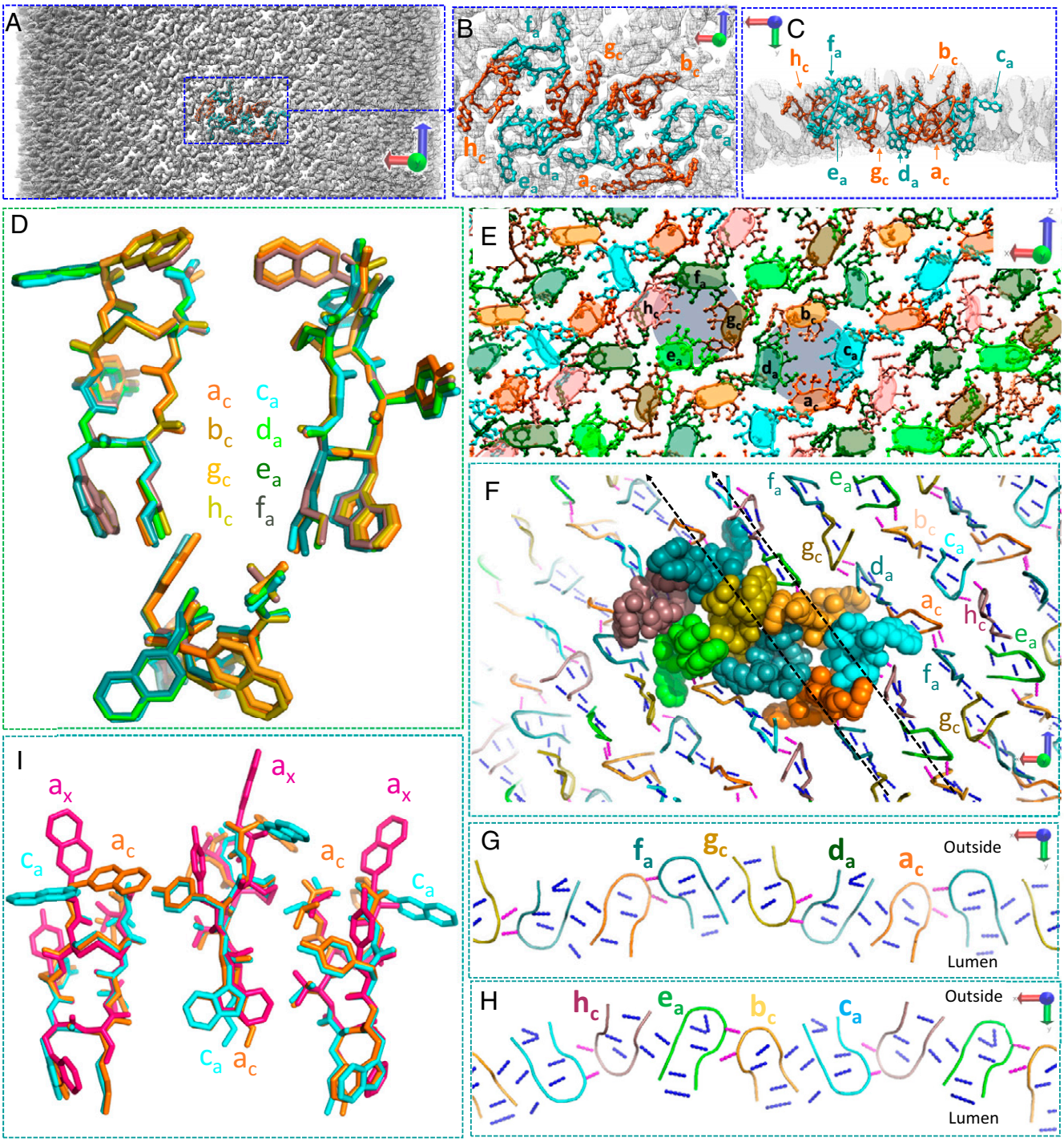

Fig. 3. Structure of Lanreotide nanotubes: (*A*) The density map for the tube, with a region outlined in the center. (*B* and *C*) Top (*B*) and side (*C*) views of the outlined region in *A* showing the density map together with the atomic model for the helical asymmetric unit. The eight molecules of the asymmetric unit are clustered into two main conformations: molecules a_c, b_c, g_c, and h_c (in orange-yellow) are capped and molecules c_a, d_a, e_a, and f_a (in cyan-green) are away. (*D*) Superposition of the eight conformations of Lanreotide found in the capped (orange) and the away (cyan) families of molecules present in the asymmetric unit. (*E*) The different environments for the eight molecules within the asymmetric unit. For clarity, the centers of the two tetramers of an asymmetric unit are highlighted with light gray circles. (*F–H*) Main-chain H-bond networks as displayed by Pymol polar contacts with default parameters. H-bonds in antiparallel β-sheets are shown as blue dotted lines and in parallel β-sheets as magenta dotted lines. (*F*) Networks as seen from outside the tube in the same orientation as *A*. One asymmetric unit is displayed as spheres and the molecules around it only by their backbones. The two black dotted lines indicate the two β-sheets shown in side views in *G* and *H*. (*G*) Side view of the β-sheet formed by molecules a_c, d_a, g_c, and f_a. (*H*) Side view of the β-sheet formed by molecules c_a, b_c, e_a, and h_c. (*I*) superposition of molecule a_c (orange) and c_a (cyan) of the asymmetric unit of the nanotubes with one of the two Lan-dap5 conformations a_x found in the crystal (magenta). The DTrp and the Tyr of the molecules forming the nanotubes are at 180° (DTrp) and 120° (Tyr) with respect to the same residues of Lanreotide in the crystal. For Nah, whereas the two conformers of Lanreotide in the nanotubes mostly differ are the level of the C_α-CH_2, (i.e., side chain conformation), the difference with the crystal is at the level of the backbone between the Carbonyl-C_α.

Downloaded from https://www.pnas.org by Universite de Rennes 1 on May 31, 2022 from IP address 129.20.30.54.

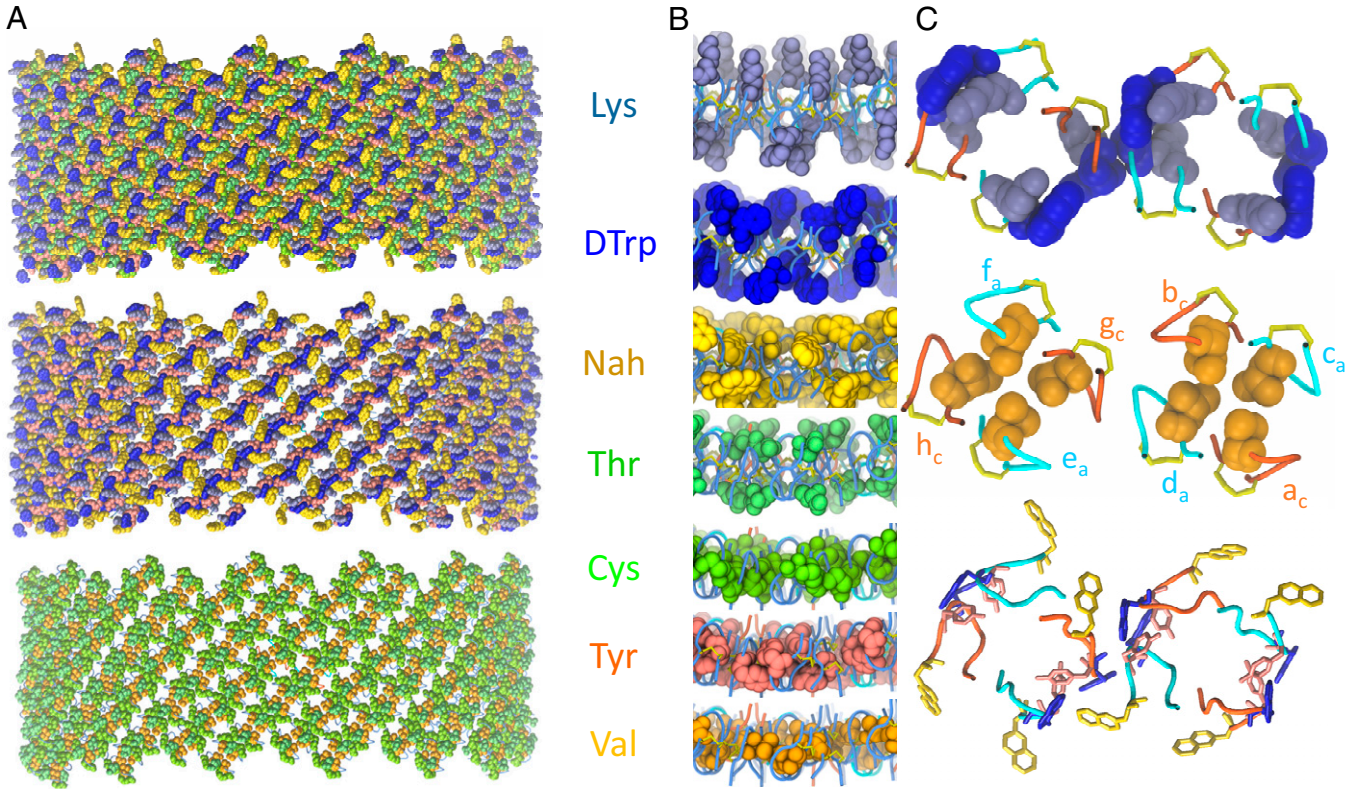

Fig. 4. Role of the side chains in the nanotube structure. (*A*) Three side views of the nanotube with either all the residues (*Top*), the aromatic residues only (*Middle*), or the aliphatic residues only (*Bottom*) shown. (*B*) Close-up of the nanotube wall: from the top to the bottom are highlighted Lys (gray blue), D-Trp (royal blue), Nah (yellow), Thr (spring green), Cys (green), Tyr (salmon), and Val (orange) residues. (*C*) Close-up of the D-Trp-Lys (*Top*), the Val cluster (*Middle*), and the aromatic stacking (*Bottom*).

does not carry any charge, as the C terminus is amidated to CO-NH2. Differing orientations of this C terminus (Fig. 3*D*) contribute to the differences between outer and luminal surfaces, for example by completing the H-bond network of β-sheets only on the luminal surface (Fig. 3 *G* and *H*).

Discussion and Conclusions

The two structures that we obtained, either by crystallography or by cryo-EM, are both at a resolution (0.83 Å and 2.5 Å, respectively) allowing for the construction of unambiguous atomic models. What is surprising is that whereas the crystal structure strongly supports the molecular model for nanotubes proposed almost 20 y ago (8), the actual cryo-EM structure of the nanotubes is fundamentally different.

This nanotube structure shows that even a small peptide has the ability to adjust to eight slightly different environments and engage in a range of similar but different interactions to self-assemble into a perfectly regular structure. This is reminiscent of the adjustments made by the much larger viral capsid proteins forming quasi-equivalent icosahedral shells. The likeness even extends to the N-terminal D-Nah of lanreotide, that resembles flexible N- or C-terminal "tails" of viral capsid proteins that feature prominently in establishing quasi-equivalent contacts (14). The resulting complexity of the nanotube structure, with eight peptides in the asymmetric unit, would be impossible to imagine from the interpretation of spectroscopic and low-resolution structural data that existed in 2003. The revolution in high-resolution cryo-EM has had a profound impact in the structural biology of large protein complexes, but is just beginning to impact assemblies of small natural and synthetic peptides (11, 15–18).

Self-assembled peptide material has important biomedical applications (1). To enable rational design of peptide material requires a deep understanding of the chemical and physicochemical rules guiding peptide assemblies and folding. However, what can be seen in many peptide assemblies is "deterministic chaos" (11), where we simply lack the tools at this point to predict how such peptides may assemble and the potentially polymorphic assemblies that may form. Since these assemblies usually result from deterministic chemical interactions, they are all potentially predictable, but we need many more structures to develop the tools needed to make such predictions. The recent success of AlphaFold (19) in predicting protein tertiary structure has depended greatly on the huge database of experimentally determined protein structures. Thus, experimental verification of models at a near-atomic level of resolution must become the standard in the area of peptide assemblies and will be an important step toward developing predictive methods.

Materials and Methods

Material. Lanreotide [H-D-2-Nal_1-cyclo(Cys_2-Tyr_3-D-Trp_4-Lys_5-Val_6-Cys_7)-Thr_8-NH2] was obtained from Ipsen Pharma and the Lan-dap5 derivatives ([H-D-2-Nal_1-cyclo(Cys_2-Tyr_3-D-Trp_4-Dap_5-Val_6-Cys_7)-Thr_8-NH2] were synthetized by solid-phase fluorenylmethyloxycarbonyl (FMOC) chemistry, as described in Tarabout et al. (9). See *SI Appendix* for analytical characterization and *SI Appendix*, Fig. S1.

Crystallization of Lanreotide Derivative Lan-Dap5. The sitting-drop method was used in 24-well plates for obtaining the Lan-dap5 crystals. The Lan-dap5 peptide powder was first solubilized in ethanol then pure water was added to the solution to reach a peptide concentration of 1.3% (wt/wt) in 50% ethanol. A 20-μL drop of the peptide solution was then equilibrated by vapor diffusion with a 500-μL reservoir of ethanol in water at a concentration from 28 to 29%.

Downloaded from https://www.pnas.org by Universite de Rennes 1 on May 31, 2022 from IP address 129.20.30.54.

The crystals attached to a surface or to each other were separated and were then salvaged with a metal loop and quickly frozen in liquid nitrogen. No additional cryoprotectant was required because of the presence of ethanol.

X-Ray Diffraction Pattern Acquisition and Analysis. Crystal X-ray diffraction data were collected on PROXIMA1 (synchrotron Soleil) beamline using a Pilatus 6M detector. Three datasets were collected at wavelengths of 0.79990 Å or 0.78971 Å and merged together. Data integration and scaling were performed using the XDS package (20). The structure of Lan-dap5 was solved by dual-space direct methods with SHELXD (21). The model was completed by alternative cycles of manual model building with Coot (22) and refinement with REFMAC5 (23). The data statistics of the Lan-dap5 structure determination are indicated in Table 1.

Cryo-EM Grid Preparation. Lanreotide powder was dissolved at 37 mM in pure water and incubated at room temperature for 24 h. Cryo-EM grids were vitrified using an FEI Vitrobot Mark IV (ThermoFisher Scientific) set at 22 °C, 100% humidity. Three microliters of nanotube sample were applied to 60-s glow-discharged Quantifoil or lacey carbon grids, blotted with filter paper for intervals of time varying between 8 and 30 s with a blotting force of 0 to 2, plunge-frozen in nitrogen-cooled liquid ethane, and stored in liquid nitrogen until data collection. The grid used for high-resolution data collection was a Lacey carbon grid blotted 15 s with a force of 0.

Image Acquisition. Movies were collected using an FEI Titan Krios microscope (300 kV) equipped with a Bioquantum/K3 energy filter/detector in counting mode. Sixty movie frames with a total dose of 60 electrons/Å^2 were recorded. Complete information on parameters of data collection and processing is given in Table 2.

Helical Reconstruction. CryoSPARC software (24) v3.2 was used for all image analysis and 3D reconstruction. Frames 2 to 40, corresponding to a total dose of 39 electrons/Å^2, were motion-corrected, dose-weighted, and summed using Patch Motion Correction. The contrast transfer function (CTF) for each aligned and summed micrograph was determined using Patch CTF estimation. Nanotube segments were automatically picked using the Filament Tracer and the Inspect Picks jobs in CryoSPARC, with a class average obtained from 172 manually picked segments as a template.

A subset containing ∼100,000 particles was randomly selected from the whole dataset and used for generating an averaged power spectrum. Indexing this power spectrum led to more than 50 possible helical symmetries. The possible symmetries were then tested in cryoSPARC, using the same subset containing 100,000 particles. The correct symmetry yielded a map with interpretable peptide-like features and apparent side-chain densities, not found for any of the other symmetries. The same symmetry was then used for helical reconstruction with the whole dataset. The final reconstruction used 2,264,921 nanotube segments extracted in boxes of 512 × 512 px at 0.85 Å/px and down-sampled to boxes of 392 × 392 px with 1.11 Å/px (Table 1). They were selected from the whole dataset (5,109,922 segments from 13,333 micrographs) after extensive 2D classification with increasingly stringent selection using cryoSPARC's class probability filter. The final reported resolution after CTF refinement on a per particle basis was 2.5 Å as judged by the map:map FSC (*SI Appendix*, Fig. S10). The resolution was not limited by the resampling from 0.85 to 1.11 Å or by the size of the box (392 × 392), as this final map was not improved by retaining the original 0.85-Å sampling or by extracting in larger boxes (640 × 640 px at 0.85 Å/px instead of the initial 512 × 512 px).

Model Building and Refinement. Model building and refinement were performed with Coot (22) and PHENIX real-space refinement (25). Both possible hands of the reconstruction were tried. One yielded an excellent fit to the density (Fig. 2) with a stereochemically convincing model (e.g., all residues in favored regions of the Ramachandran plot without Ramachandran restraints applied in refinement) (Table 2). In contrast, the other hand yielded a model with very poor stereochemistry (e.g., most residues as Ramachandran outliers even with Ramachandran restraints applied) despite a suboptimal fit to density in places. Both problems were linked to strains in the model around C_α centers (Fig. 2 *E*, *Right*). No secondary structure, NCS, or Ramachandran restraints were used in refinement.

Data Availability. The atomic coordinates for the X-ray model have been deposited in the Protein Data Bank, https://www.rcsb.org/ (PDB ID code 7Q5G). The cryo-EM atomic model, map, and images have been deposited in the PDB (ID code 7Q5A), Electron Microscopy Data Base, https://www.ebi.ac.uk/emdb/ (EMD-13830), and Electron Microscopy Public Image Archive, https://www.ebi.ac.uk/empiar/ (EMPIAR 10873).

ACKNOWLEDGMENTS. We thank the staff of the computing facility of Service Informatique et Calcul Scientifique at Institute for Integrative Biology of the Cell (I2BC) for their help; and our chemist colleagues Bernard Rousseau, deceased this year, and Jean-Christophe Cintrat for the synthesis of Lan-dap5. This work has been partly done on different facilities: the Transmission Electron Microscopy-Team in Commissariat à l'Energie Atomique Saclay for preliminary negative staining images; the Cryoelectron Microscopy facility of I2BC and the Nanoimaging Core at Institut Pasteur. This work was supported by The 'French Infrastructure for Integrated Structural Biology' ANR-10-INSB-05-01 and NIH GM122510 (to E.H.E.) and K99GM138756 (to F.W.). Ipsen Biopharmaceuticals is acknowledged for providing us with Lanreotide-acetate.

1. T. L. Lopez-Silva, J. P. Schneider, From structure to application: Progress and opportunities in peptide materials development. *Curr. Opin. Chem. Biol.* **64**, 131–144 (2021).
2. H. Acar *et al.*, Self-assembling peptide-based building blocks in medical applications. *Adv. Drug Deliv. Rev.* **110-111**, 65–79 (2017).
3. M. S. Khan, F. El-Khouly, P. Davies, C. Toumpanakis, M. E. Caplin, Long-term results of treatment of malignant carcinoid syndrome with prolonged release Lanreotide (Somatuline Autogel). *Aliment. Pharmacol. Ther.* **34**, 235–242 (2011).
4. O. Alexopoulou *et al.*, Efficacy and tolerability of lanreotide Autogel therapy in acromegalic patients previously treated with octreotide LAR. *Eur. J. Endocrinol.* **151**, 317–324 (2004).
5. B. Gutt *et al.*, Four-year follow-up of acromegalic patients treated with the new long-acting formulation of Lanreotide (Lanreotide Autogel). *Exp. Clin. Endocrinol. Diabetes* **113**, 139–144 (2005).
6. E. Pouget *et al.*, Elucidation of the self-assembly pathway of lanreotide octapeptide into beta-sheet nanotubes: Role of two stable intermediates. *J. Am. Chem. Soc.* **132**, 4230–4241 (2010).
7. C. Valéry *et al.*, Self-association process of a peptide in solution: From beta-sheet filaments to large embedded nanotubes. *Biophys. J.* **86**, 2484–2501 (2004).
8. C. Valéry *et al.*, Biomimetic organization: Octapeptide self-assembly into nanotubes of viral capsid-like dimension. *Proc. Natl. Acad. Sci. U.S.A.* **100**, 10258–10262 (2003).
9. C. Tarabout *et al.*, Control of peptide nanotube diameter by chemical modifications of an aromatic residue involved in a single close contact. *Proc. Natl. Acad. Sci. U.S.A.* **108**, 7679–7684 (2011).
10. F. Gobeaux *et al.*, Directing peptide crystallization through curvature control of nanotubes. *J. Pept. Sci.* **20**, 508–516 (2014).
11. F. Wang *et al.*, Deterministic chaos in the self-assembly of β sheet nanotubes from an amphipathic oligopeptide. *Matter* **4**, 3217–3231 (2021).
12. E. H. Egelman, F. Wang, Cryo-EM is a powerful tool, but helical applications can have pitfalls. *Soft Matter* **17**, 3291–3293 (2021).
13. J. Hattne *et al.*, Analysis of global and site-specific radiation damage in cryo-EM. *Structure* **26**, 759–766.e4 (2018).
14. S. C. Harrison, A. J. Olson, C. E. Schutt, F. K. Winkler, G. Bricogne, Tomato bushy stunt virus at 2.9 A resolution. *Nature* **276**, 368–373 (1978).
15. F. Wang *et al.*, Structural analysis of cross α-helical nanotubes provides insight into the designability of filamentous peptide nanomaterials. *Nat. Commun.* **12**, 407 (2021).
16. E. H. Egelman *et al.*, Structural plasticity of helical nanotubes based on coiled-coil assemblies. *Structure* **23**, 280–289 (2015).
17. Z. Feng, *et al.*, Artificial intracellular filaments. *Cell Rep. Phys. Sci.* **1**, 100085(2020).
18. S. A. Hughes *et al.*, Ambidextrous helical nanotubes from self-assembly of designed helical hairpin motifs. *Proc. Natl. Acad. Sci. U.S.A.* **116**, 14456–14464 (2019).
19. J. Jumper *et al.*, Highly accurate protein structure prediction with AlphaFold. *Nature* **596**, 583–589 (2021).
20. W. Kabsch, XDS. *Acta Crystallogr. D Biol. Crystallogr.* **66**, 125–132 (2010).
21. G. M. Sheldrick, A short history of SHELX. *Acta Crystallogr. A* **64**, 112–122 (2008).
22. A. Casañal, B. Lohkamp, P. Emsley, Current developments in coot for macromolecular model building of electron cryo-microscopy and crystallographic data. *Protein Sci.* **29**, 1069–1078 (2020).
23. G. N. Murshudov *et al.*, REFMAC5 for the refinement of macromolecular crystal structures. *Acta Crystallogr. D Biol. Crystallogr.* **67**, 355–367 (2011).
24. A. Punjani, J. L. Rubinstein, D. J. Fleet, M. A. Brubaker, cryoSPARC: Algorithms for rapid unsupervised cryo-EM structure determination. *Nat. Methods* **14**, 290–296 (2017).
25. P. V. Afonine *et al.*, Real-space refinement in PHENIX for cryo-EM and crystallography. *Acta Crystallogr. D Struct. Biol.* **74**, 531–544 (2018).
26. P. V. Afonine *et al.*, New tools for the analysis and validation of cryo-EM maps and atomic models. *Acta Crystallogr. D Struct. Biol.* **74**, 814–840 (2018).

Downloaded from https://www.pnas.org by Universite de Rennes 1 on May 31, 2022 from IP address 129.20.30.54.